JOURNAL OF PROPULSION AND POWER
Vol. 24, No. 6, November–December 2008

Contrarotating Turbine Aerodesign for an Advanced Hypersonic Propulsion System

Guillermo Paniagua* and Szabolcs Szokol†
von Karman Institute, 1640 Rhode Saint Genèse, Belgium
Hiromasa Kato‡ and Giovanni Manzini§
Cenaero, 6041 Gosselies, Belgium
and
Richard Varvill¶
Reaction Engines, Ltd., Abingdon, England OX14 3DB, United Kingdom

DOI: 10.2514/1.35612

Contrarotating turbomachinery is part of a novel airbreathing system to power a vehicle from takeoff to hypersonic speeds. The turbine-based combined cycle precools the inlet air before compression, with the hydrogen fuel as the heat-rejection sink. To ensure a safe engine operation, a helium loop is introduced between the air and hydrogen cycles; the helium drives the turbines of the main turbocompressor. The high speed of sound and low compressibility of the helium results in subsonic blading with low divergence of the endwalls. This paper describes in detail the aerodesign procedure of contrarotating helium turbines, which allows a net reduction in turbine size while augmenting the turbine efficiency. The design methodology is reviewed starting from the preliminary velocity triangle analysis. Studies were conducted to determine the effect over efficiency, outlet swirl and periodicity of the blade height, degree of reaction, and work distribution. The three-dimensional optimizer demands efficient parameterization techniques to account for the lean/sweep/twist geometry. The present multidisciplinary design includes the calculation of the centrifugal stresses. Three different helium turbine architectures have been designed and optimized, with special care to ensure an adequate performance at offdesign operation, and particular attention was devoted to minimize the secondary flows.

Nomenclature

a	=	speed of sound, m/s ($\sqrt{\gamma \cdot \Re \cdot T}$)
C	=	chord of the airfoil, m
C_p	=	specific heat, J/kg · K
H	=	enthalpy, J
h	=	specific enthalpy, J/kg
I	=	moment of inertia, kg · m^2
M	=	real Mach number (a/V)
M_{is}	=	isentropic Mach number
P	=	pressure, Pa
p	=	power, W
R	=	radius, m
$\Re$	=	ideal gas constant, J/kg · K
Re	=	mainstream Reynolds number ($\rho \cdot V_2 \cdot C/\mu$)
S	=	curvilinear abscissa along the surface, m
T	=	temperature, k
U	=	$\omega \times R$ rotor peripheral velocity, m/s
V	=	absolute velocity, m/s
W	=	relative velocity, m/s
α	=	absolute flow angle, deg
β	=	relative flow angle, deg
γ	=	heat capacity ratio, isentropic exponent [$C_p/(C_p - \Re)$]
η	=	efficiency, %
μ	=	dynamic viscosity, kg/(m · s)
ϕ	=	stage flow factor (V_{ax}/U)
Ψ	=	stage loading factor ($\Delta H/U^2$)
ω	=	rotational speed, rad/s

Subscripts

ax	=	projection along the turbine axis
is	=	isentropic conditions
LE	=	leading edge
r	=	frame of reference relative to rotor
s	=	static conditions
TE	=	trailing edge
0	=	absolute conditions
1	=	vane inlet conditions
2	=	rotor inlet conditions
3	=	rotor outlet conditions

Presented as Paper 1341 at the 28th International Symposium on Airbreathing Engines, Beijing, China, 2–7 September 2007; received 11 November 2007; revision received 22 May 2008; accepted for publication 29 June 2008.

*Assistant Professor, Turbomachinery and Propulsion Department, Chaussée de Waterloo 72; paniagua@vki.ac.be. Member AIAA.
†Research Engineer, Turbomachinery and Propulsion Department, Chaussée de Waterloo 72.
‡Research Scientist, Batiment Mermoz, Avenue Jean Mermoz 30. hiromasa.kato@cenaero.be.
§Research Scientist, Batiment Mermoz, Avenue Jean Mermoz 30. giovanni.manzini@cenaero.be.
¶Technical Director, Building D5, Culham Science Centre; Richard.varvill@reactionengines.co.uk.

I. Introduction

HIGH-SPEED long-range vehicles should operate at low velocity during takeoff and at hypersonic velocity at cruise conditions. Balepin [1] has recently reviewed several synergistic propulsion cycles based on airbreathing concepts. Reaction Engines, Ltd. [2] has developed a turbine-based combined-cycle engine (named Scimitar) intended for Mach 5 antipodal cruise. Figure 1 presents the layout of the thermodynamic cycle, which serves as a good example in our design methodology. The subsonic and supersonic performances are ensured by incorporating a high bypass fan into the bypass duct, which encloses the core engine and is otherwise needed to match the intake-air-capture flow to the engine-demanded flow over the supersonic Mach number range. The bypass

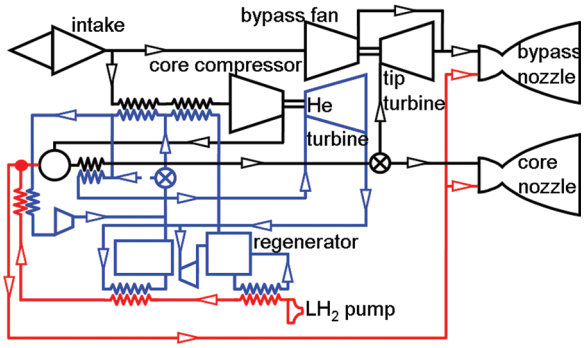

Fig. 1 Scimitar basic cycle layout of air (in black), helium (in blue), and liquid hydrogen (LH_2, in red).

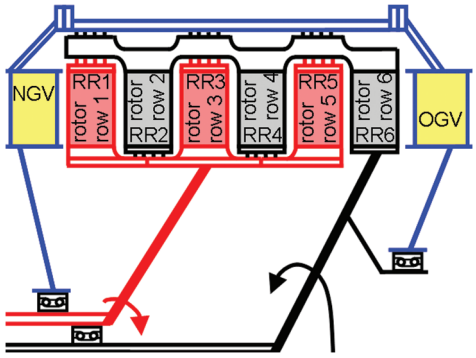

Fig. 2 Counter-rotating turbine layout with the successive rotor rows (RR) and final outlet guide vane (OGV).

fan is driven by a hub turbine using flow diverted from the core engine nozzle. The flow then discharges into the bypass and mixes with the bypass flow. At Mach 5 precooling allows high compression rates, enhancing the engine thrust-to-weight ratio. The oxygen required for the combustion of hydrogen fuel in the expansion nozzle is taken from the atmosphere, cooled down in a heat exchanger, and subsequently compressed in the axial compressor. In a parallel closed helium cycle, the heat exchanger provides the enthalpy rise before the expansion in the helium turbine that drives the main air compressors.

Helium is the selected energy carrier in several pilot nuclear power plants (where weight is not an issue) because of its chemical inertness and high energy density [3,4]. The C_p of helium is 4.5 times that of air; thus, the temperature drop in a helium turbine is 4.5 times lower for an identical enthalpy drop. The heat capacity ratio γ of helium is 20% higher than that of air; hence, the pressure ratio in a helium turbine is about 20 times lower. The pressure and temperature changes are very small along the machine axis, and so the blade height remains nearly unaltered. The turbine geometries developed for gas turbines could not be simply scaled for helium. To ensure similarity between prototypes and models, the testing gas ought to have the same isentropic exponent [5], a possible solution would be the use of argon. Because of the high C_p and γ, the speed of sound in a helium turbine is 3 times higher than in a conventional one. As a consequence, in all the studied designs, the flow is subsonic (the maximum Mach number remains below 0.65). Currently, there are several ongoing projects on high-temperature reactors with a direct closed cycle using helium as a working fluid [6–8].

Contrarotating turbines (CRTs) have successive blade rows that spin in opposite directions, as depicted in Fig. 2. Such a configuration reduces the size and weight, eliminates gyroscopic effects, and reduces cooling requirements. At the advent of gas turbine propulsion, Griffith [9] had already realized the superiority of counter- above corotation. Wintucky and Stewart [10] showed the overall efficiency levels for variations in work and speed ratio for a two-shaft turbine. The two shafts of the turbine can then be linked to a contrarotating compressor machine or toward two independent conventional compressors, counter-rotating. Garnier [11] proposed the use of variable-stagger guide vanes to control the relative load in the compressor. Louis [12] studied two cases with and without nozzle guide vane (NGV) with two contrarotating rotors considering identical rotational speed. The comparison with a conventional high-reaction turbine revealed that similar stage loading factors Ψ can be achieved with lower rotor turning, resulting in higher efficiencies (3% in the proposed example). Cai et al. [13] carried out a comprehensive study of the possible contrarotating configurations to be selected (degree of reaction and inlet and outlet flow angles) as a function of the imposed velocity and work distribution among the rotors. According to Sotsenko [14], in helicopter gas turbines, statorless contrarotating designs allow a temperature increase of about 60 K.

CRTs evidence technical challenges that prevented their extensive use. The mechanical design is particularly complex: bearings rotating at high peripheral speeds, unconventional assemblies, and high seal-leakage flows. Daniels et al. [15] measured large-windage torque in adjacent rotating disks; it was proposed to reduce it by adding a diaphragm between the disks. Davidson and Finke [16] described the construction of a setup to perform experiments of a contrarotating version of the space shuttle's main engine turbopump; however, no data are provided on the turbine details or flow analysis. Keith et al. [17] presented the efficiency variability as a function of the pressure ratio, proving the superiority of a vaneless CRT. The blade-row interactions are an important source of tonal noise [12], mechanical excitations [18,19], and pulsating heat fluxes [20]. A particular concern in the development of any engine is the blade gust due to the unsteady shock and wake-row interactions. Some recent numerical studies address wake interactions [21] and hot-streak migration [22], but further research is required to gain more valuable physical insight. Future research directions would tackle clocking investigations in CRTs with an equal number of airfoils in the corotating blade rows.

In the current paper, the initial architecture was composed of six rotor blade rows. The one-dimensional flowpath was optimized for several turbine configurations. Emphasis was placed on the mean-annulus design phase, as 90% of the cost and weight of the turbine gas engines is determined in this preliminary phase [23]. Studies have been conducted to find the most efficient design with favorable outlet swirl and blade-row acceleration. The parameters to adjust were the blade height, degree of reaction, work distribution across the stages, blade-row acceleration, and blade number. No turbine had intermediate stator blade rows. In parallel with the aerodynamic optimization, the mechanical integrity of the airfoils was assessed. The blade stresses and displacements were computed using a finite element model (FEM) solver. On the final four-rotor-row configuration, several multirow computations using a time-averaged 3-D Navier–Stokes (N-S) simulation have been carried out to estimate the turbine performance at offdesign conditions.

II. Design Methodology

A. Turbine-Stage Definition

Figure 3 displays the velocity triangles in a 3-rotor-row turbine. The first stage is a conventional turbine stage comprising a vane plus a rotor blade row, as described in turbomachinery textbooks (for instance, see Saravanamuttoo et al. [24]). The outlet flow of rotor row 1 ($V_{3_{RR1}}$) has a rather high swirl, and that converted into the relative frame of the second rotor row is rather small ($W_{2_{RR2}}$), thanks to the contrarotation. In turbines with corotating rotors, a stator vane is required to deflect the flow in the sense of rotation to reduce the rotor inlet velocity in the subsequent blade rows.

Although there are no vanes between the rotor rows in Fig. 3, let us consider a *phantom* vane of infinitely small chord and zero turning. Stage 2 and all subsequent stages are therefore composed of a phantom vane and a real rotor. This assumption allows the use of conventional design tools, with different signs in the rotation of each turbine stage. Figure 3 (bottom) presents the velocity triangles in stage 3.

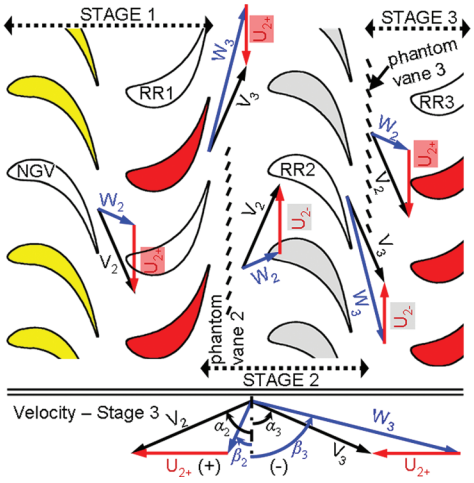

Fig. 3 Velocity triangles in a 3-rotor-row CRT.

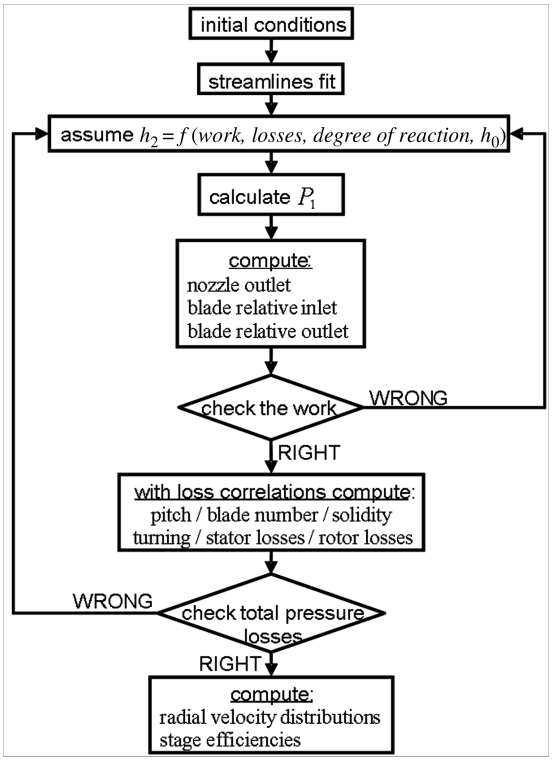

Fig. 4 Flowchart of the Meanline-Streamline Analysis Program.

B. Preliminary Annulus Design

This is a critical part of the process, as 80% of the final product is decided in the first 20% of the design time [25]. Because of the novel characteristics of the current specifications, the design process started from scratch using velocity triangles, Smith [26] charts, and simple correlations based on the required power, maximum rotational speed, and available space for the turbine. The pitch-to-chord ratios have been determined using the correlation of Dejc and Trojanovskij [27], which is a function of the inlet and outlet flow angles, trailing-edge thickness, and outlet Mach number.

The primary optimization of the detailed turbine geometry (variation of blade height and flow angles) is made by means of the Meanline-Streamline Analysis Program [28], for which the flowchart is shown in Fig. 4. This performance-prediction method is based on the equations of radial equilibrium. It makes use of the different turbine correlations for profile, secondary flow, clearance, and gap losses to predict the turbine performance. The results presented here are obtained with the correlations of Soderberg (described in [29]). The program predicts the flow variation from hub to shroud at all sections between the stators and rotors and estimates the performance (work output and efficiency). Applying this program to different geometries allows defining the optimum combination of flow angles and blade height over the different turbine stages.

C. Two-Dimensional Blade Design

An inverse design tool [30] was then used to define blade sections with a smooth acceleration in the suction side up to the throat. The input data are the inlet flow angle, stagger angle, pitch-to-chord ratio, and a preliminary pressure distribution. The program starts with the analysis of a first guess of the blade geometry by means of a potential flow solver. The difference between the calculated and required velocity is used as an input for the modification algorithm based on a transpiration technique. This provides a new blade shape for which the velocity distribution is now closer to the desired one. The process is repeated until the calculated velocity distribution matches the requirements. A major advantage of this method is its very short design cycle and easy offdesign analysis. In the present case, with Mach numbers sometimes below 0.3 (incompressible flow), this solver can yield good preliminary blades.

The output of the inverse design is a blade contour defined by a series of points that is then fitted with Bezier curves (Fig. 5, left). Bezier curves allow a compact parameterization of the geometry, with an easy update of curvature degree. Although inflexion points can occur, they are far less frequent than with polynomials. Once the airfoil is described by Bezier curves, an N-S simulation is launched. Figure 5 (right) shows that the N-S solution agrees well with the potential (inviscid) flow calculation.

Afterward, the optimum parameters of the 2-D airfoil profiles were obtained using a 2-D neural-network solver and a genetic algorithm (GA) [31], as described in Fig. 6. The artificial neural network is used to find the approximate relation between the parametric geometry: aerodynamic boundary conditions on one side, and the aerodynamic performance on the other side. The optimizer is the GA that finds the blade design that gives the best performance.

D. Three-Dimensional Aerodynamic Analysis

A 3-D geometry is obtained by stacking (in the radial direction) the optimum 2-D sections along their center of gravity. The performance is then analyzed by means of the multistage 3-D N-S solver TRAFMS [32]. The Reynolds-averaged N-S equations are solved using a Runge–Kutta scheme in conjunction with accelerating techniques (e.g., multigrid). The equations are discretized using finite volumes and a cell-centered scheme with second- and fourth-order artificial dissipation. The blade-to-blade grid-generation process is based on an elliptic procedure that solves the discretized Poisson equations using a point-relaxation scheme. The three-dimensional grid is generated by stacking the two-dimensional nonperiodic grids. The two-layer Baldwin–Lomax mixing-length model is used to compute the turbulent quantities. The flow is assumed to be turbulent all along the blade surface and endwalls. Each blade row is modeled with 315,000 nodes; that is, in the

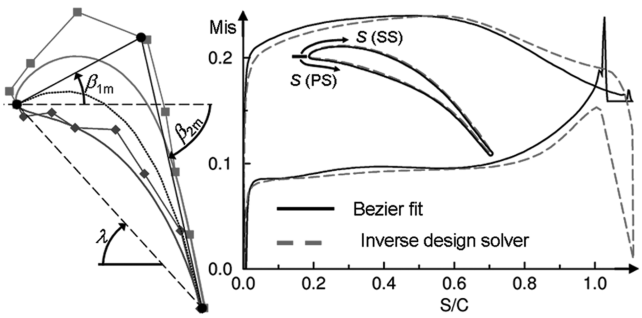

Fig. 5 Bezier fit of an airfoil for the N-S simulation (left) and comparison of the velocity distribution predicted by the inverse design solver solution with the N-S solution along the suction side (SS) and pressure side (PS) (right).

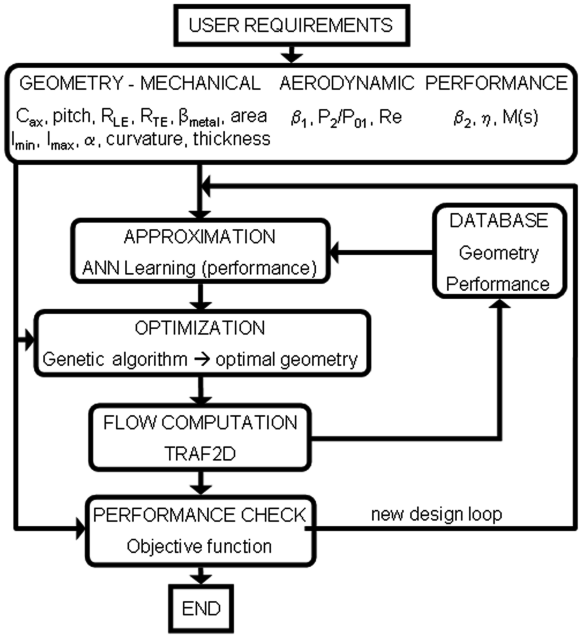

Fig. 6 Flowchart of the blade optimization algorithm (ANN is an artificial neural network).

four-turbine study, the five blade rows are coupled using the mixing-plane approach (1.6 million nodes).

E. Mechanical-Stress Calculation

The nodes of the computational fluid dynamics (CFD) grid on the blade surface are not appropriate for FEM computations. Additionally, the CFD does not model the fillet at the blade endwall. A new blade definition is produced using four nonuniform rational B-splines. A fillet radius of 1 mm is used on both the pressure and suction sides. The blade definition is then imported to SAMCEF software. Tetrahedral elements are used for the meshing, refined close to the fillets. The main solicitation in the blades is the tensile stress caused by the centrifugal acceleration. Because the turbine-inlet temperature to the uncooled airfoils is below 1000 K, thermal stresses are expected to be low.

F. Three-Dimensional Optimization Algorithm

The methodology is based on a GA significantly accelerated by the use of an approximate model. The approach has numerous advantages, such as the capability to easily couple multidisciplinary and multipoint simulations. The method has demonstrated an excellent ability to cope with a complex objective function space, such as the one displayed in Fig. 7, with many local minima. Aerodynamic analysis is performed by solving the flowfield at three different operating points with TRAFMS, and structural constraints such as maximum stress and natural frequencies are imposed to the FEM. The blade shape is parameterized by B-spline control points at three spanwise locations, the B-spline curve defining the lean, and

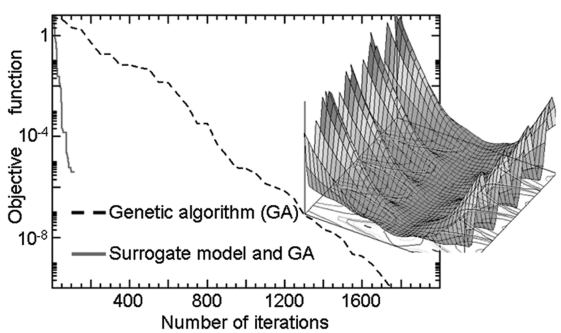

Fig. 7 Performance of the optimization method.

the number of blades per row. This results in the design space consisting of both continuous and discrete parameters, which can pose a problem for gradient-based optimization algorithms. Moreover, the number of design variables can easily approach 50 or 100, which explains the tremendous effect on the computational cost. These requirements justify the use of a GA combined with surrogate models.

The optimization algorithm is organized in five steps:

1) A database is built using a design of experiments (DOE) procedure; numerous techniques exist: full factorial, fractional, central composite, D-optimal, Latin-hypercube, and random selection, among others.

2) An approximate model is built using the DOE points to construct an analytical relation between the design variables and the simulation responses.

3) An optimization algorithm is used to find the optimum using the approximate model to evaluate the objective functions and constraints.

4) The accurate simulation is used to evaluate and verify the real objective function and constraint values. This new simulation result is added to the database. The database is therefore continuously improved with new design points, thereby leading to an improved approximate model.

5) Go to step 2 until the maximum number of optimization iterations specified by the user is reached.

In this study, the design of experiments is performed using a random selection of design points, with special care taken to ensure the maximum coverage of the design space. This optimizer [33] is parallelized using message passing interface protocol. In general, the number of design points generated in the DOE is about 2 to 5 times the number of design variables. The generated samples are used to construct a surrogate model based on the radial-basis-function network.

An inappropriate choice of parameterization can lead to a significant increase in the number of optimization iterations to reach the optimum or, worse, failure to achieve improvement in a practical amount of time. The number of design parameters must be as small as possible. The set of design parameters must be able to generate a wide spectrum of feasible configurations. These are inherently conflicting requirements, and thus it is not a trivial issue. Each blade was parameterized by three airfoil sections, and each section was parameterized by camberline, stagger angle, and axial chord scaling factor. The camberline is expressed as a B-spline curve, hierarchically parameterized for compactness. Along with the number of blades, this results in 40 design parameters for the problem.

G. Optimization Problem

The objective function F of the optimization is a weighted sum of the efficiencies at 3 operating conditions ($F = \eta_1 + 0.5\eta_2 + 0.5\eta_3$), where η_1 is the on-design efficiency, and η_2 and η_3 are the efficiencies at offdesign mass-flow conditions. Thus, the objective is to maximize this function subject to the constraints. The motivation behind multipoint optimization is to ensure that the final geometry also performs reasonably well at offdesign conditions. In fact, automatic optimization often tends to overoptimize at a particular operating condition if no offdesign information was fed back in the evaluation of the objective function. Ideally, one should employ robust design techniques to alleviate such a problem, but in the current study, a simple weighted-sum approach was deemed satisfactory enough, and it will be shown later that it is indeed the case in the performance-map comparison.

The aerodynamic constraints were placed on the outlet swirl angle as well as the mass flow. The swirl angle was constrained to be 30 deg at maximum, and the mass-flow rate was strictly constrained at the nominal design value. The total power output was also constrained to be at its nominal value. On the other hand, the distribution of extracted power among two counter-rotating spools was left free, and the baseline turbine had the identical power output from each spool. For each design candidate (individual), a structural FEM grid was

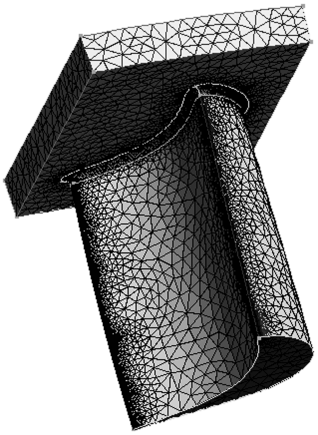

Fig. 8 Typical FEM mesh.

automatically constructed, with a 1 mm fillet added to the supporting endwall, as shown in Fig. 8. The static-stress analysis was performed by SAMCEF software. A centrifugal force corresponding to the rotational speed was applied to the structure. Two materials were used in the analysis: steel alloy and high-temperature plastic, from which appropriate maximum von Mises stresses are computed and subsequently constrained during the optimization.

H. Turbine Boundary Conditions

The requested shaft power in each axis is around 32 MW, and the axes counter rotate at around 11,000 rpm. The helium mass flow available is about 90 kg/s, with a mean diameter of around 250 mm. The turbine-inlet total pressure and temperature are 20×10^6 Pa and 1000 K. The lifetime requirement is 40,000 h.

III. Two-Rotor-Row and Three-Rotor-Row Turbines

A. Two-Rotor-Row Monodimensional Design

A configuration with only two rotor rows, each delivering 32 MW, is the most compact machine, with a very high stage loading factor ($\Psi \approx 4.4$). Figure 9 (top left) sketches the configuration with two rotor rows, in which the power is transmitted directly to the two rotor discs.

Figure 10 presents how the turbine outlet swirl changes with the nozzle-guide-vane outlet flow angle and the acceleration rate through the blade row or ratios of outlet to inlet relative Mach numbers M_{3r}/M_{2r}. Axial outlet flow is obtained when $\alpha_{2\,\text{stage}\,1} = 0$. On the other hand, the flow on the second stage is decelerated ($M_{3r}/M_{2r} < 1$), which is unacceptable. The optimum $\alpha_{2\,\text{stage}\,1}$ is 68 deg, which ensures acceleration rates across both stages $M_{3r}/M_{2r} > 2$. The flow turning is 130 deg, which will result in high secondary flows and very poor total-to-static efficiency ~68% (88% total to total). The turbine outlet swirl can be reduced to only 5 deg by requesting 30% less work of the second rotor row and increasing the work extraction in the first stage by the same amount. The resulting

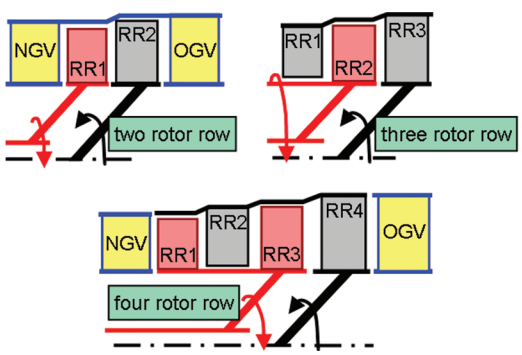

Fig. 9 Three different CRT architectures for a two-shaft machine: two, three, and four stages.

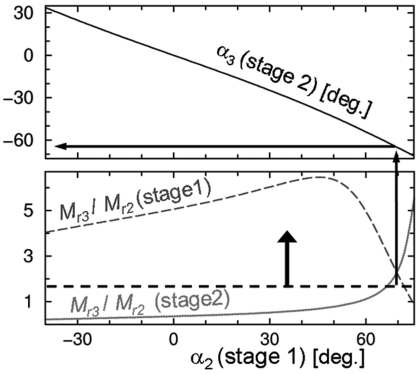

Fig. 10 Turbine outlet swirl as a function of the inlet-vane outlet flow angle (top) and acceleration across the rotor in the first and second stages (bottom).

total-to-static efficiency is 82% (total to total is lower: 87%), with the first rotor row turning equal to 138 deg. A compromise solution is to increase the power extraction and rpm by 5% in stage 1. The total-to-static efficiency is rather low (~71%), with a turbine exit swirl of 63 deg, which requires a downstream deswirler.

B. Three-Rotor-Row Monodimensional Design

Playing with the work distribution, it is possible to eliminate the NGV and ensure a minimum blade-row acceleration of 1.7, while achieving a low turbine outlet swirl (~10 deg.). Figure 9 (top right) presents a sketch of the turbine; the first rotor row is overhung on the turbine casing. This design requires only 3 blade rows, with a stage loading factor Ψ ranging between 1.7 and 4.7. In spite of the high turning required in the second rotor row (about 130 deg), the total-to-static efficiency is 88% (total to total is 92%). The turning in the first and third rotor rows are 23 and 85 deg, respectively. The acceleration rates M_{3r}/M_{2r} across the successive three rotor rows are 3.2, 1.4, and 1.4.

IV. Four-Rotor-Row Architecture

A. Velocity Triangles

A four-rotor-row turbine (Fig. 9, bottom) was designed to further increase the turbine efficiency. First, the possibility of using the same airfoil in the four blade rows was investigated (i.e., similar velocity triangles in all stages). To achieve this, the relative work distribution between the blade rows fixed to the same axis was varied. In Fig. 11, the abscissa is the percent of work difference between stage 1 and stage 3, and the ordinate is the percent of work difference between the second and last stages. The relative inlet flow angles to the blades of the first and second stages are imposed to be identical. Figure 11 (top) shows that the vane outlet flow angle and degree of reaction in the second stage are unaffected by the work distribution between stages 2 and 4. A configuration with identical inlet flow angle to the second and third rotor rows is represented by the diagonal area. To also guarantee the same inlet flow in the third and fourth rotor rows, the work distribution must be nearly the same in all rotor rows (represented with the dotted ellipse). In this area of operation, the turbine outlet swirl is above 52 deg, which would imply that the total-to-static efficiency will be strongly penalized.

To limit the development cost of the turbine, the next alternative investigated is to have only periodic conditions in each axis. Namely, blade rows 1 and 3 have the same velocity triangles, whereas in the second shaft, blade rows 2 and 4 are similar. The optimum configuration in terms of efficiency has a constant flow factor ϕ and stage loading Ψ of 0.6 and 2.1, respectively. The turbine exit swirl is 29 deg, the total-to-static efficiency is 91.4% (the total to total 94.8%), and acceptable acceleration rates M_{3r}/M_{2r} range between 1.6 and 3.2. Figure 12 sketches the layout of the optimum turbine. If the rotational speed would be decreased by 10%, the relative inlet flow angle to the first rotor row would be reduced by 5 deg Thus,

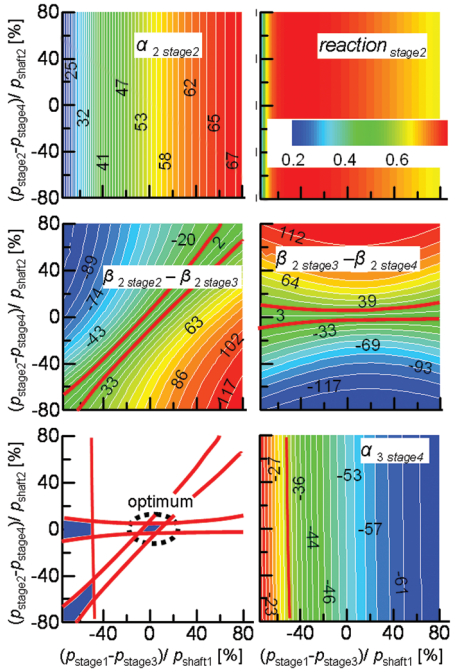

Fig. 11 Periodicity analysis of the 4-stage turbine as a function of the power distribution among the two stages in each shaft.

blades able to perform without separation at a ± 10 deg incidence are suitable to ensure a good offdesign operation.

B. Design of the NGV in the First Stage

The design of an efficient NGV was difficult due to the low turning (31 deg) with little increase in the Mach number from inlet to outlet (0.09 to 0.11). Once the 2-D design was completed using the inverse code, different chord-to-pitch ratios were analyzed to balance the global loss with the performance of each individual airfoil. A 2-D optimizer provided several solutions that were analyzed to ensure that no separation bubble appeared in at the rear suction side. The design was done robustly enough to guarantee that the blade performed well at ± 5 deg of incidence. For the positive incidence case, the Mach number distribution showed a peak in the front suction side, because the stagnation point was shifted to the pressure side, which forces the flow to accelerate. Nevertheless, the flow remained attached around the leading edge. For the -5 deg incidence angle, the blade performs well.

Initially, the blade was radial, stacked along the leading edge. The analysis of the 3-D flowfield revealed very weak secondary flows. Therefore, lean will not reduce the losses; however, different lean configurations were investigated to obtain a more uniform outlet flowfield. Figure 13 displays how the optimum lean of 7 deg results in a more uniform outlet flow angle. The hub section moves into a lower-velocity region (higher pressure), whereas the tip moves into a higher-velocity region. Thus, the blade loading is reduced at the hub

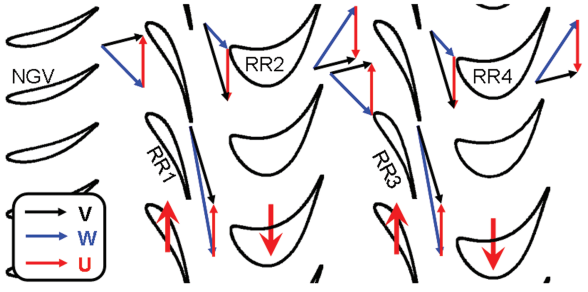

Fig. 12 Four-rotor-row turbine: aerodesign of the blades and velocity triangles.

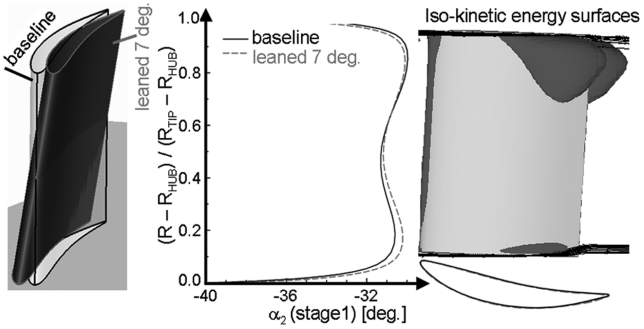

Fig. 13 Baseline stator versus the lean geometry.

and increased at the tip, which results in a negative spanwise gradient along the suction surface from hub to tip. For completeness, iso-kinetic-energy surfaces were used to visualize the very weak secondary flows constrained at the rear suction side close to the endwalls. The 3-D final geometry is prismatic: no compound is implemented, due to the weakness of the secondary flows. The same 2-D profile is used from hub to tip.

C. Design of the Blade in the First Stage

In the rotor, three sections were designed at the hub, midspan, and tip. Figure 14a displays the shape of the airfoil at midspan. Note that the required turning is only 30 deg. The obtained airfoil has a rather smooth acceleration until the throat at $S/S_{\max} = 0.65$ (Fig. 14b). It is interesting to note that Mamaev and Khramin [34] experimentally verified that for such low turning blades, positive incidences have minimum losses, whereas for conventional airfoils, a negative incidence is beneficial.

The optimum geometry does not change along the span, as shown in Fig. 14c. Once the 3-D geometry was defined, stress calculations were performed considering that the blade material is Jethete M152. The blade in stage 1 is attached to the hub platform. Figure 15 (left) shows that maximum levels of stresses ($\sim$130 MPa) are reached along the fillet region.

By contrast, rotor row 2 is attached to the casing (as sketched in Fig. 9, bottom). The maximum stresses ($\sim$200 MPa) are obtained again along the suction side of the fillet (Fig. 15, right). The rest of the airfoils have been designed in a similar manner. In counter-rotating turbines, there are high concerns regarding how small variations in the flow angle from one rotor row affect the following blade rows [35]. In the present case, if the relative outlet flow angle of stage 1 varies by 1 deg, the relative inlet angle of the second blade row changes by 2.2 deg. Therefore, rotor rows 2, 3, and 4 were designed to withstand variations in the incidence of ± 10 deg.

D. Three-Dimensional Multirow Analysis

Three-dimensional multirow calculations were performed in the five blade rows to study the flow behavior. The growth of the

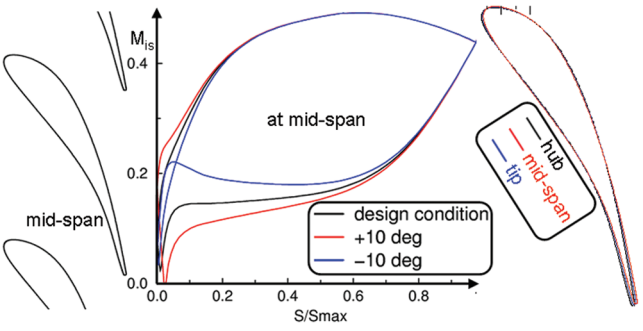

Fig. 14 Blade of stage 1 at the midspan geometry (a), velocity distribution at the midspan (b), and geometry at the hub and tip (c).

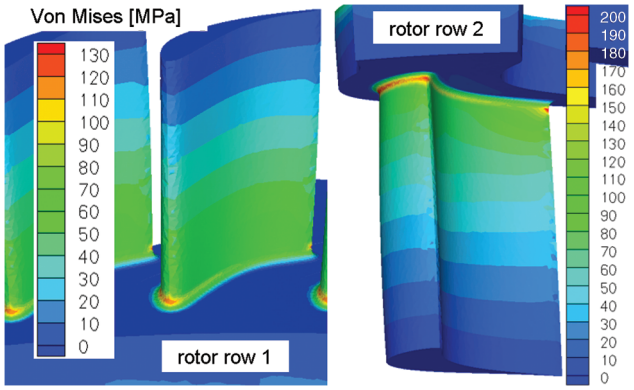

Fig. 15 Blade stress calculations in the first and second stages.

boundary layer and secondary-flow development across the stages imply that the radial inlet conditions from stage to stage are not uniform. Calculations were run at five different pressure ratios at 5 rpm (8000 to 12,000) to characterize the performance map of the designed turbine. Figure 16 shows a view of the turbine stage with the grid used in the calculation. The calculation requires 1500 iterations to converge and nearly 70 h of CPU time on an alpha station DEC 500 5/333.

The skewness caused to the boundary layer by the counter-rotation helps to obtain a more homogenous flow-angle distribution from one blade row to the next. Indeed, the fourth rotor row has a very similar radial distribution of inlet flow angle to that of the second rotor row. The relative inlet flow angle changes only by 4 deg from hub to tip.

Figure 17 presents the total-to-static isentropic efficiency. Increasing the rotational speed raises the efficiency; additionally, the efficiency becomes less insensitive to variations in the mass flow. At

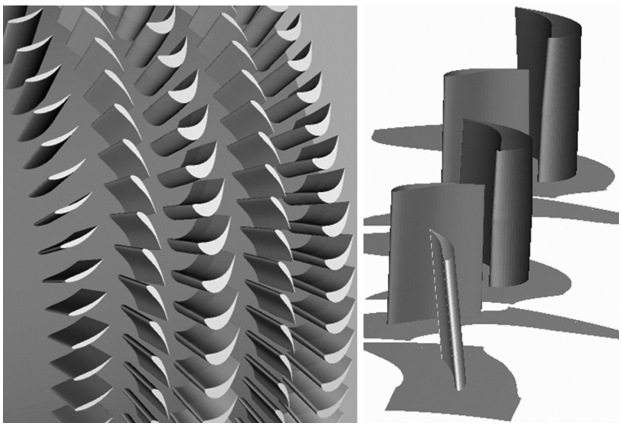

Fig. 16 Three-dimensional views of the final four-stage turbine.

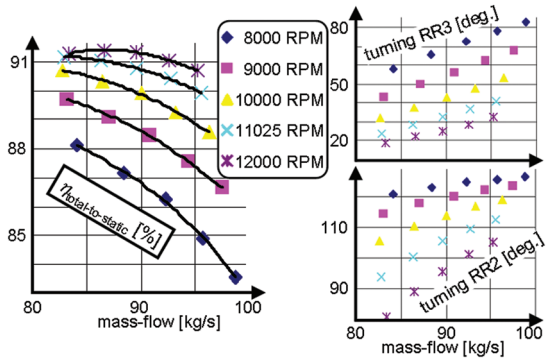

Fig. 17 Turbine total-to-static efficiency and blade turning at various mass flows and rpm.

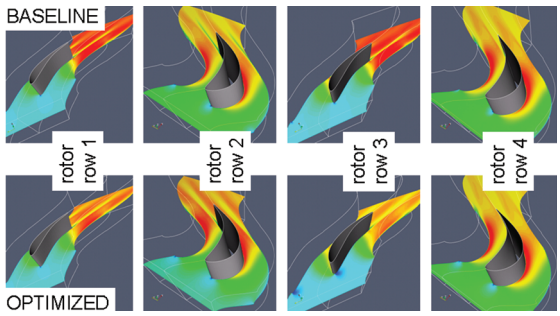

Fig. 18 Midspan Mach number contours of the baseline and optimized for the four-blade airfoils.

nominal rpm, the efficiency continuously decreases with the mass flow from 91.2 to 89.9%. By changing the mass flow (by adjusting the pressure ratio) or the rpm, the incidences to the blades are changed, whereas the rotor outlet relative angle is little affected. Figure 17 (right) shows the turning of the second and third rotor rows for the different conditions. The turning in rotor rows 2 and 4 is nearly identical, whereas the variations in stage 1 are much lower than in stage 3. When the mass flow increases, the incidence increases (toward negative values) in the first and third rotor rows, resulting in an increased turning. Similarly, in rotor rows 2 and 4, the turning increases with the mass flow. In consequence, at the maximum mass flow, the flow separates in the blade crown. By reducing the rpm, the turning is increased, which explains the reduction in efficiency.

E. Three-Dimensional Optimization

The preliminary design of the turbine was outlined in the previous sections. The airfoil sections and turbine configuration were parameterized as discussed previously. The average computational time for a design candidate took about 2.5 h, which was the time it took to do a single CFD run. The structural analysis was performed in parallel to the CFD simulations. First, the DOE run was carried out with 130 samples, about 3 times the number of design parameters. The surrogate-model-based optimization was run up to 200 iterations, beyond which no significant increase in performance was observed.

Figure 18 shows Mach number contours at the midspan plane for both baseline and optimized turbines. The blade pitch comparison is shown in Table 1. The efficiency of the optimized turbine is improved across a range of operating conditions and, on average, an approximate 0.5% increase in efficiency was uniformly achieved. It should also be noted that the total number of blades was reduced, indirectly leading to a reduction in weight, although the weight was not explicitly part of the optimization problem.

For brevity, only the result of the structural analysis on the optimized blade is shown in Fig. 19 for stages 3 and 4, manufactured in Jethete M512. The maximum von Mises stress constraints are safely satisfied. One of the less obvious benefits of multidisciplinary optimization, such as this study, is that the constraints can be formulated in a more natural manner. For example, without the presence of structural analysis, one would typically have to constrain minimum thickness at certain geometric points. Though this seems a minor issue, this kind of geometric constraint often degrades the convergence of optimization. Thus, it is more beneficial to formulate such constraints based on physical terms, rather than on ad hoc geometric terms. This is indeed one of the advantages of using GA as the core of optimization, as it allows us to treat the objective function evaluation purely as a black box.

Table 1 Comparison of blade pitches

	Rotor row 1	Rotor row 2	Rotor row 3	Rotor row 4
Baseline	90	84	96	91
Optimized	88	86	87	86

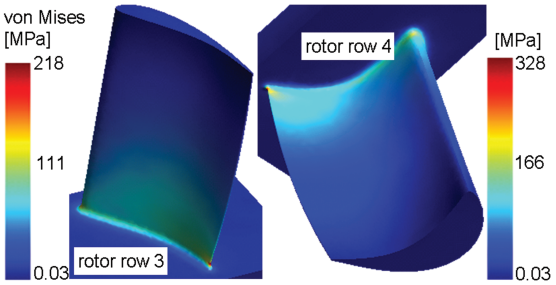

Fig. 19 Von Mises stress for the optimized rotor rows 3 and 4 manufactured in Jethete M512.

V. Conclusions

This paper presents a complete methodology to design and optimize contrarotating turbines. Various possible configurations for a counter-rotating turbine were analyzed. The numerical analysis comprised a mean line design for the definition of the aerodynamic and thermodynamic properties of the flow, a two-dimensional design of the blades, a three-dimensional optimization, and a stress calculation. In spite of the mechanical complexity of CRTs, their performance is superior to conventional turbines, not only because stator blade rows are eliminated, but also because the blade rows can be designed with lower turning. The chosen solution is a balance between maximum efficiency/acceleration across the blade row/periodicity and minimum turbine exit swirl. The constraints to respect were that the turning should not exceed 130 deg, the size of the machine should be kept small, and the periodicity across the stages should be guaranteed to simplify the blade design. The following parameters were evaluated: number of stages, blade height, degree of reaction, work distribution across the stages, and rotational speed. A decrease in the number of stages results in lower efficiency, high turnings, and high turbine outlet swirl. Furthermore, to reestablish the periodicity in the velocity triangles, it is necessary to decrease the degree of reaction. Once the number of stages is fixed, higher levels of the degree of reaction result in higher efficiency values.

The NGV of the 4-rotor-row turbine turns the flow only 31 deg (in conventional turbines, this value ranges between 65 and 73 deg). The proposed three-rotor-row turbine does not have an NGV. This very compact design may, however, encounter problems during the startup. CRTs demonstrate a more complex flow behavior across the stages than conventional turbines, leading to high offdesign conditions that should be assessed.

Once the airfoils were optimized in 2-D sections, the 3-D geometry was obtained by staking the sections along the radial direction. On this baseline geometry, 3-D 5-row calculations were performed to evaluate the design and offdesign operation. With a 3-D optimization, the efficiency was further increased by changing the pitch and the shape while reducing the variability of the efficiency with the mass-flow changes. The optimized geometry had fewer blades and hence less weight. Finally, the stress calculations demonstrate that the mechanical constraints are respected.

Acknowledgments

This work was performed within the Long-Term Advanced Propulsion Concepts and Technologies (LAPCAT) project investigating high-speed airbreathing propulsion. LAPCAT is supported by the European Union within the 6th Framework Programme, Priority 1.4, Aeronautic and Space, contract no. AST4-CT-2005-012282, and is coordinated by ESA's European Space Research and Technology Centre. The authors would like to acknowledge Tom Verstraete for developing the methodology to perform the stress calculations. Special thanks to Abdelkader Benyahia for his assistance in the three-dimensional analysis of the vane and multirow calculations.

References

[1] Balepin, V., "High Speed Propulsion Cycles," *Advances on Propulsion Technology for High-Speed Aircraft*, RTO/AVT/VKI Lecture Series, von Karman Inst. for Fluid Dynamics, Rhode-Saint-Genèse, Belgium, Mar. 2007.

[2] Bond, A., "Turbine Based Combined Cycles," *Advances on Propulsion Technology for High-Speed Aircraft*, RTO/AVT/VKI Lecture Series, von Karman Inst. for Fluid Dynamics, Rhode-Saint-Genèse, Belgium, Mar. 2007.

[3] Bammert, K., Krey, G., and Küper, K. D., "Performance of High-Temperature Reactors with Helium Turbines," International Atomic Energy Agency Paper SM-111/14, 1969.

[4] Bammert, K., and Deuster, G., "Layout and Present Status of the Closed-Cycle Turbine Plant in Oberhausen," American Society of Mechanical Engineers Paper 74-GT-132, 1974.

[5] Roberts, S. K., and Sjolander, S. A., "Effect of the Specific Heat Ratio on the Aerodynamic Performance of Turbomachinery," *Journal of Engineering for Gas Turbines and Power*, Vol. 127, No. 4, Oct. 2005, pp. 773–780. doi:10.1115/1.1995767

[6] Ballot, B., "Presentation of the Present HTR Concepts and Large Associated Facilities," *High Temperature Reactor School (HTR/ECS 2002)*, 2002, https://odin.jrc.ec.europa.eu/htr-tn/HTR-Eurocourse-2002/Ballot_562.pdf.

[7] McDonald, C. F., Adams, R. G., Bell, F. R., and Fortescue, P., "Component Design Considerations for Gas Turbine HTGR Power Plant," American Society of Mechanical Engineers Paper 75-GT-67, 1975.

[8] Muto, Y., Ishiyama, S., Tanuma, T., Kishibe, T., and Matsumoto, I., "Design Study of Helium Turbine for the 600 MWt HTGR-GT Power Plant," *Proceedings of the International Gas Turbine Congress*, Vol. 1, 1999, pp. 313–320.

[9] Griffith, A. A., "Contrarotating Axial Flow High and Low Pressure Turbine and Compressor with Bladed Duct with Turbine Cooling," U.S. Patent No. 2,477,798, 1948.

[10] Wintucky, W. T., and Stewart, W. L., "Analysis of Two Stage Counter-Rotating Turbines Efficiencies in Terms of Work and Speed Requirements," NACA RM E57L05, 1958.

[11] Garnier, M. R., "Improvements in or Relating to Gas Turbine Engines Having Contrarotating Compressors," London Patent No. 1,146,347, 1969.

[12] Louis, J. F., "Axial Flow Contra-Rotating Turbines," American Society of Mechanical Engineers Paper 85-GT-218, 1985.

[13] Cai, R., Wu, W., and Fang, G., "Basic Analysis of Counter-Rotating Turbines," American Society of Mechanical Engineers Paper 90-GT-108, 1990.

[14] Sotsenko, Y. V., "Thermogasdynamic Effects of the Engine Turbines with the Contra-Rotating Rotors," American Society of Mechanical Engineers Paper 90-GT-63, 1990.

[15] Daniels, W. A., Johnson, B. V., and Graber, D. J., "Aerodynamic and Torque Characteristics of Enclosed Co/Counterrotating Rotors," *Journal of Turbomachinery*, Vol. 113, No. 1, 1991, pp. 67–74. doi:10.1115/1.2927739

[16] Davidson, D. P., and Finke, A. K., "The Design and Fabrication of a Small Highly Counterrotating Turbine Rig," American Society of Mechanical Engineers Paper 93-GT-396, 1993.

[17] Keith, B. D., Basu, D. K., and Stevens, C., "Aerodynamic Test Results of Controlled Pressure Ratio Engine Dual Spool Air Turbine Rotating Rig," American Society of Mechanical Engineers Paper 2000-GT-632, 2000.

[18] Weaver, M. M., Manwaring, S. R., Abhari, R. S., Salay, M. J., Frey, K. K., and Heidegger, N., "Forcing Function Measurements and Predictions of a Transonic Vaneless Counter Rotating Turbine," American Society of Mechanical Engineers Paper 2000-GT-0375, 2000.

[19] Haldeman, C. W., Dunn, M. G., Abhari, R. S., Johnson, P. D., and Montesdeoca, X. A., "Experimental and Computational Investigation of the Time-Averaged and Time-Resolved Pressure Loading on a Vaneless Counter-Rotating Turbine," American Society of Mechanical Engineers Paper 2000-GT-445, 2000.

[20] Dunn, M. G., Haldeman, C. W., Abhari, R. S., and McMillan, M. L., "Influence of Vane/Blade Interaction Spacing on the Heat Flux for a Transonic Turbine," *Journal of Turbomachinery*, Vol. 122, No. 4, Oct. 2000, pp. 684–691. doi:10.1115/1.1313818

[21] Qingjun, Z., Huishe, W., Xiaolu, Z., and Jianzhong, X., "Numerical Analysis of 3-D Unsteady Flow in a Vaneless Counter-Rotating Turbine," *Frontiers of Energy and Power Engineering in China*, Vol. 1,

No. 3, July 2007, pp. 352–358.
doi:10.1007/s11708-007-0053-3

[22] Qingjun, Z., Huishe, W., Xiaolu, Z., and Jianzhong, X., "Numerical Investigation on the Influence of Hot Streak Temperature Ratio in a High-Pressure Stage of Vaneless Counter-Rotating Turbine," *International Journal of Rotating Machinery*, Vol. 2007, Paper 56097, 2007.
doi:10.1155/2007/56097

[23] Gregory, B. A., "Considerations for the Aerodynamic Optimization of a Turbine," *Turbomachinery Blade Design Systems*, VKI Lecture Series, von Karman Inst. for Fluid Dynamics, Rhode-Saint-Genèse, Belgium, Nov. 1999.

[24] Saravanamuttoo, H. I. H., Rogers, G. F. C., and Cohen, H., *Gas Turbine Theory*, 5th ed., Prentice–Hall, New York, 2001.

[25] Taylor, M., "HP Axial Flow Turbine Aerodynamic Design," *Advances in Turbomachinery Aero-Thermo-Mechanical Design and Analysis*, VKI Lecture Series, von Karman Inst. for Fluid Dynamics, Rhode-Saint-Genèse, Belgium, Nov. 2006.

[26] Smith, S. F., "A Simple Correlation of Turbine Efficiency," *The Journal of the Royal Aeronautical Society*, Vol. 69, No. 655, July 1965, p. 467.

[27] Dejc, M. E., and Trojanovskij, B. M., "Untersuchung und Berechnung Axialer Turbinenstufen," VEB Verlag Technik, Berlin, 1973.

[28] De Michele, C., MacDonald, P., and Sieverding, C., "Meanline-Streamline Analysis Program," von Karman Inst. for Fluid Dynamics, Rept. PR1975-13, Rhode-Saint-Genèse, Belgium, 1975.

[29] Sieverding, C., "Axial Turbine Performance Prediction Methods," *Thermodynamics and Fluid Dynamics of Turbomachinery*, Vol. 1, NATO Advanced Studies Inst., Series E, No. 97A, 1985, pp. 737–784.

[30] Leonard, O., and Van den Braembussche, R. A., "Design Method for Subsonic and Transonic Cascades with Prescribed Mach Number Distribution," *Journal of Turbomachinery*, Vol. 114, No. 3, July 1992, pp. 553–560.
doi:10.1115/1.2929179

[31] Pierret, S., and Van den Braembussche, R. A., "Turbomachinery Blade Design Using a Navier-Stokes Solver and Artificial Neural Network," *Journal of Turbomachinery*, Vol. 121, No. 2, 1999, pp. 326–332.
doi:10.1115/1.2841318

[32] Arnone, A., Liou, M.-S., and Povinelli, L. A., "Navier-Stokes Solution of Transonic Cascade Flows Using Non-Periodic C-Type Grids," *Journal of Propulsion and Power*, Vol. 8, No. 2, 1992, pp. 410–417.

[33] Pierret, S., Filomeno-Coelho, R., and Kato, H., "Multidisciplinary and Multiple Operating Points Shape Optimization of Three-Dimensional Compressor Blades," *Journal of Structural and Multidisciplinary Optimization*, Vol. 33, No. 1, 2007, pp. 61–70.
doi:10.1007/s00158-006-0033-y

[34] Mamaev, B. I., and Khramin, R. V., "About Choice of Incidence at Designed Turbine Cascade," *Proceedings of the 6th World Conference on Experimental Heat Transfer, Fluid Mechanics, and Thermodynamics (ExHFT-6)* [CD-ROM], Apr. 2005, Paper 4-b-6.

[35] Cheng, J. L., "Analysis of Technical Challenges In Vaneless Counter-Rotating Turbomachinery," American Society of Mechanical Engineers Paper 2007-GT-27617, 2007.

L. Maurice
Associate Editor